Computer Assisted Methods in Engineering and Science
32(3): 255–270, 2025, https://doi.org/10.24423/cames.2025.1729

Application of the Finite Pointset Method to Numerical Modeling of Heat Transfer in Two-dimensional Tissue Subjected to a Moving Laser Beam

Anna KORCZAK[1)*], Felix R. SAUCEDO-ZENDEJO[2)]

[1)] *Silesian University of Technology, Faculty of Mechanical Engineering, Department of Computational Mechanics and Engineering, Gliwice, Poland*

[2)] *Universidad Autónoma de Coahuila, Centro de Investigacion en Matemáticas Aplicadas, Saltillo, México; e-mail: fesaucedoz@uadec.edu.mx*

[*] *Corresponding Author e-mail: anna.korczak@polsl.pl*

In this article, a numerical analysis of thermal processes occurring in biological tissue during laser irradiation is presented. The mathematical model is based on the two-dimensional Pennes equation. The analyzed tissue is exposed to the laser irradiation of a moving beam with constant velocity along the tissue surface. The upper face of the skin tissue is subjected to the vertical laser beam, and it is assumed that heat dissipation through convection and radiation from the surface is negligible compared to the heat delivered by the laser beam. Thus, the surface is treated as thermally insulated surface. The effect of the laser beam's transitional speed and power on the temperature distribution within the skin tissue are investigated. Moreover, the perfusion rate and the effective scattering coefficient are treated as variables dependent on tissue damage. In the computational part of this study, the finite pointset method (FPM) is applied. The temperature distribution computed with FPM is compared with an analytical one obtained for a three-dimensional problem by analyzing a relevant cross-section under the same conditions. This modeling of the dynamic thermal processes within biological tissue subjected to laser irradiation supports the evaluation of biological tissue damage and provides a basis for determining the time and intensity of laser irradiation. In the last part of the article, numerical examples and conclusions are presented.

Keywords: finite pointset method, meshless methods, laser irradiation, moving laser beam, Pennes equation.

1. Introduction

Heat transfer within living tissue is a complex process involving conduction in a heterogeneous medium, blood perfusion through the tissue, and metabolic

heat generation. Several mathematical models, nowadays including very advanced three-phase lag bioheat models, have been proposed and studied to understand the biological heat transfer within skin tissue [1]. Among these models, the Pennes model [2], thermal wave models [3], and the dual-phase lag model are the most commonly used [4]. In the literature, numerous studies have addressed the solution of heat transfer equations in skin tissue, particularly under the influence of stationary or moving laser beams. An example is presented in the work of Askarizadeh and Ahmadikia [5], where the authors derived an analytical solution for both Fourier and non-Fourier bioheat equations. They incorporated metabolic heat generation and blood perfusion rate in a two-dimensional skin tissue model subjected to laser heat flux. Based on the available literature, most studies have focused on modeling stationary laser beams, while only a limited number of investigations have addressed moving single-point laser beams. For example, Partovi *et al.* [6] solved numerically the Fourier and non-Fourier governing equations for three-dimensional case by using the standard finite element method (FEM). Their results compare the thermal response of tissue under moving single-point and multi-point laser.

Therefore, the application of the finite pointset method (FPM) to model heat transfer in biological tissue is proposed in this article. The heat transfer model is based on the transient two-dimensional Pennes equation [7]. Furthermore, the research delves into the influence of laser irradiation from a moving beam, using an approach based on Beer's law, which delineates the attenuation of laser energy as it passes through tissue [8]. The model assumes that the perfusion rate and the effective scattering coefficient vary with tissue injury, along with the energy ratio delivered by the laser. In this study, simplified boundary conditions with assigned fixed temperature values of 37°C at the corresponding boundaries are considered. This temperature, representing the inner layer of skin tissue, is assumed to be the same for all considered boundaries. The rationale behind this simplification is to reduce computational burden and to align our approach with a reference solution [6], enabling straightforward comparison of results. Such a comparison is essential for assessing the applicability of numerical techniques to novel problems, including the one addressed here. The authors are aware that this approach does not fully capture the complexity of real physiological conditions. To better represent heat transfer in biological tissue, future work will consider a three-layer skin model. In addition, parameter variations found in the literature will be replaced with fuzzy parameters to account for uncertainties and enhance the realism of the simulation.

The use of meshless methods in modeling bioheat transfer is not popular in the literature. In particular, the FPM method remains a novel approach and represents a contribution to the development of numerical methods for heat flow with potential medical applications. To the best of the authors' knowl-

edge, this study is the first to apply FPM to two-dimensional bioheat problems. This method relies on the weighted least-squares technique to estimate spatial derivatives and solve elliptic partial differential equations. Several studies have explored FPM applications in other areas of mechanics, including fluid mechanics [9], radiative [10] and conductive heat transfer problems [11], and linear elasticity-related issues [12]. Notably, one of the key advantages of this meshless approach is its capacity to handle complex geometries and irregular boundaries [11]. Unlike traditional FEM or finite difference method, FPM does not require a structured mesh. Instead, it utilizes a scattered set of points distributed across the domain, showcasing exceptional flexibility in handling intricate geometrical configurations, and even time-varying geometries. Additionally, mesh-based approaches prove inadequate for addressing issues related to extensive mesh deformations, dynamic discontinuities, or scenarios necessitating constant remeshing throughout the solution process due to their inherent high computational costs. In response to these challenges, meshless methods have emerged as viable alternatives, offering potential solutions to alleviate some of the limitations associated with traditional mesh-based methodologies.

The structure of the paper is as follows: Sec. 2 shortly describes the Pennes equation, Sec. 3 presents the fundamental concepts behind the two-dimensional FPM and it is numerical implementation for solving the Pennes equation. Numerical examples are presented in Sec. 4. Finally, conclusions and directions for future work are given in the last section.

2. The Pennes equation

This section presents the Pennes bioheat partial differential equation, along with appropriate boundary and initial conditions, as the mathematical framework for modeling temperature distribution in biological tissues exposed to different heat sources, particularly laser irradiation from a moving beam with constant velocity. The basic form of the Pennes equation in the two-dimensional domain is given as follows [13]:

$$c\frac{\partial T}{\partial t}(x,y,t) = \lambda\left(\frac{\partial^2 T}{\partial x^2}(x,y,t) + \frac{\partial^2 T}{\partial y^2}(x,y,t)\right) + Q_{\text{perf}} + Q_{\text{met}} + Q_{\text{las}}, \quad (1)$$

where λ [$\mathrm{W}\cdot\mathrm{m}^{-1}\cdot\mathrm{K}^{-1}$] is the thermal conductivity, c [$\mathrm{J}\cdot\mathrm{m}^{-3}\cdot\mathrm{K}^{-1}$] is the volumetric specific heat, T [°C] is the temperature, t [s] is the time, x and y [m] denote spatial coordinates, and $Q_{\text{perf}}, Q_{\text{met}}, Q_{\text{las}}$ [$\mathrm{W}\cdot\mathrm{m}^{-3}$] are heat sources due to blood perfusion, metabolic activity and laser irradiation, respectively.

The laser heat source considered in this study is defined as [6]:

$$Q_{\text{las}}(x,y,t) = 2\varepsilon\mu_t' Q_1(x,t)Q_2(y), \quad (2)$$

where 2ε [m] is the width of the laser beam cross-section (Fig. 1), μ_t' [m^{-1}] is the attenuation coefficient, $Q_1(x,t)$ and $Q_2(y)$ [$\mathrm{W}\cdot\mathrm{m}^{-3}$] are the heat distribution of the laser in the x- and y-directions, respectively. The laser's impact cross-section is modeled as an interval, representing a reduction of three-dimensional square of size $2\varepsilon \times 2\varepsilon$, moving at a speed v along the tissue in the x-direction. Thus, $Q_1(x,t)$ and $Q_2(y)$ based on Beer's law [14] can be written as:

$$Q_1(x,t) = \delta\left[x - (vt + x_s)\right], \tag{3}$$

$$Q_2(y) = (1 - Rf)I_0 \exp\left(-\mu_t' y\right), \tag{4}$$

where Rf [ ] and I_0 [$\mathrm{W}\cdot\mathrm{m}^{-2}$] are the light reflection coefficient and the laser power, respectively. In the simulations, the initial beam center is taken as point $(x_s,\ y_s)$ and it is the location of the laser beam at time $t = 0$ (in the numerical calculations this point is taken as (0, 0)). The function $\delta(x)$ defines the irradiation region by limiting it to an interval and is given by:

$$\delta(x) = \begin{cases} 0, & x > \varepsilon, \\ \dfrac{1}{2\varepsilon}, & -\varepsilon < x < \varepsilon, \\ 0, & x < -\varepsilon. \end{cases} \tag{5}$$

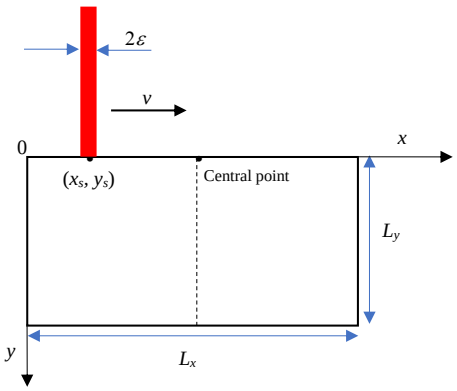

FIG. 1. Schematic of a two-dimensional skin tissue exposed to a moving laser beam.

The attenuation coefficient is defined as:

$$\mu_t' = \mu_a + \mu_s', \tag{6}$$

where μ_a [m^{-1}] is the absorption coefficient and μ_s' [m^{-1}] is the effective scattering coefficient, which is treated as a function of tissue injury represented by the Arrhenius integral:

$$\mu_s'(\theta = \mu_{s\,\mathrm{nat}}' \exp(-\theta) + \mu_{s\,\mathrm{den}}' \left(1 - \exp(-\theta)\right). \tag{7}$$

The injury Arrhenius integral is defined as [15]:

$$\theta(x,y,t^F) = \int_0^{t^F} A \exp\left[-\frac{\Delta E}{RT(x,y,t)}\right] dt, \tag{8}$$

where A [s^{-1}] is the pre-exponential factor, ΔE [$\mathrm{J}\cdot\mathrm{mol}^{-1}$] is the activation energy of the reaction, R [$\mathrm{J}\cdot\mathrm{mol}^{-1}\cdot\mathrm{K}^{-1}$] is the universal gas constant, and t^F [s] is the duration of thermal exposure. For parameter values, see Table 4.

The perfusion heat source function taken into account is as follows:

$$Q_{\mathrm{perf}}(x,y,t,\theta) = c_B G_B\left(\theta(x,y,t)\right)\left(T_B - T(x,y,t)\right), \tag{9}$$

where G_B [$\mathrm{m}^3_{\mathrm{blood}}\cdot\mathrm{s}^{-1}\cdot\mathrm{m}^{-3}_{\mathrm{tissue}}$] is the blood perfusion rate, c_B [$\mathrm{J}\cdot\mathrm{m}^{-3}\cdot\mathrm{K}^{-1}$] is the volumetric specific heat of blood, while T_B [°C] denotes the arterial blood temperature. The blood perfusion coefficient is a function determined based on the tissue necrosis and is modeled as a polynomial function [15]:

$$G_B(\theta(x,y,t)) = G_{B0}\sum_{j=1}^{3} m_j \theta(x,y,t)^{j-1}, \tag{10}$$

where m_j are specified coefficients (see Sec. 4), G_{B0} is the initial blood perfusion coefficient, and θ is the value of the injury integral.

To effectively model heat conduction, it is crucial to establish a suitable set of boundary and initial conditions tailored to the specific problem outlined earlier in this section. These conditions are considered as follows:

$$T(0,y,t) = T_{b1}, \tag{11}$$

$$T(L_x,y,t) = T_{b2}, \tag{12}$$

$$T(x,L_y,t) = T_{b3}, \tag{13}$$

$$-\lambda\frac{\partial T}{\partial y}(x,0,t) = q_b, \tag{14}$$

$$T(x,y,0) = T_0. \tag{15}$$

The proposed mathematical model, which incorporates a moving laser beam and parameters dependent on the injury integral, provides a more precise depiction of the heat transfer process within living tissue compared to models based on constant values in the standard Pennes equation.

3. The FPM for the two-dimensional problem

The FPM is a meshless, Lagrangian, strong-form approach that employs a weighted least-squares interpolation technique to approximate spatial derivatives [16]. This method for solving partial differential equations is based on the Taylor series expansion, facilitating the calculation of a function and its spatial derivatives, which act as unknown coefficients within the series. Detailed implementation guidelines for the FPM are available in various literature sources [17–19]. In this section, the main concepts of the FPM are presented, with a particular focus on its application to the two-dimensional Pennes equation.

Let Ω be a given domain with a particular boundary, generally considered in three-dimensional space. Suppose a set of points $x_1, x_2, ..., x_n$ is distributed with corresponding function values $T(x_1), T(x_2), ..., T(x_n)$. The objective is to find an approximate value of the function T at some arbitrary location x. For this purpose, let us define the approximation of $T(x_j)$ using the Taylor series expansion around x:

$$T_{\text{aprox}}(x_j) = T(x) + \sum_{k=1}^{3} T_k(x) dx_j^k + \frac{1}{2} \sum_{k,l=1}^{3} T_{kl}(x) dx_j^k dx_j^l. \tag{16}$$

The unknown values $T(x)$, $T_k(x)$, $T_{kl}(x)$, $(k = 1, 2,\ l = 1, 2)$ are obtained using a weighted least squares method by minimizing the quadratic expression while considering all neighboring points (np):

$$J = \sum_{j=1}^{np} w_j (\mathbf{Ma} - \mathbf{b})^2. \tag{17}$$

After some mathematical operations, the minimization of function J yields the formal solution:

$$\mathbf{a} = (\mathbf{M}^T \mathbf{W} \mathbf{M})^{-1} (\mathbf{M}^T \mathbf{W}) \mathbf{b}, \tag{18}$$

where

$$w(x_j, x) = \begin{cases} \exp\left(-\beta \left\|x_j - x\right\|^2 / h^2\right), & \left\|x_j - x\right\| \le h, \\ 0, & \text{otherwise}, \end{cases} \tag{19}$$

and

$$\mathbf{W} = \begin{pmatrix} w(x_1, x) & 0 & \cdots & 0 \\ 0 & w(x_2, x) & 0 & 0 \\ \vdots & \vdots & \ddots & \vdots \\ 0 & 0 & \cdots & w(x_{np}, x) \end{pmatrix}, \tag{20}$$

where β is a positive constant. The value of h defines a set of neighboring points around x. At this point, we assume that x belongs to the interior part of Ω. For two-dimensional case, the matrix $\mathbf{M}$, the unknown vector $\mathbf{a}$, and the vector $\mathbf{b}$ are defined as follows:

$$\mathbf{M} = \begin{pmatrix} 1 & dx_1^1 & dx_1^2 & \frac{1}{2}\left(dx_1^1\right)^2 & dx_1^1 dx_1^2 & \frac{1}{2}\left(dx_1^2\right)^2 \\ 1 & dx_2^1 & dx_2^2 & \frac{1}{2}\left(dx_2^1\right)^2 & dx_2^1 dx_2^2 & \frac{1}{2}\left(dx_2^2\right)^2 \\ \vdots & \vdots & \vdots & \vdots & \vdots & \vdots \\ 1 & dx_{np}^1 & dx_{np}^2 & \frac{1}{2}\left(dx_{np}^1\right)^2 & dx_{np}^1 dx_{np}^2 & \frac{1}{2}\left(dx_{np}^2\right)^2 \\ 2c & 0 & 0 & -\lambda\Delta t & 0 & -\lambda\Delta t \end{pmatrix}, \tag{21}$$

$$\mathbf{a} = [T(x), T_1(x), T_2(x), T_{11}(x), T_{12}(x), T_{22}(x)]^t, \tag{22}$$

$$\mathbf{b} = \left[T^{\tau+1}(x_1), T^{\tau+1}(x_2), ..., T^{\tau+1}(x_{np}), 2\Delta t Q^\tau + 2cT^\tau(x) + \lambda\Delta t\nabla^2 T^\tau(x)\right]^t. \tag{23}$$

The FPM operates as an iterative technique, where the vector $\mathbf{a}$ in Eq. (18) is recomputed for each particle.

It is worth mentioning that if the point x lies on the boundary of Ω and satisfies either the second or third type of boundary conditions, an additional row must be added to matrix (21) and corresponding element to vector (23) to impose such a boundary condition. For the Neumann boundary condition $\left(-\lambda\frac{\partial T}{\partial n} = q_b\right)$ we have:

$$\mathbf{M} = \begin{pmatrix} 1 & dx_1^1 & dx_1^2 & \frac{1}{2}\left(dx_1^1\right)^2 & dx_1^1 dx_1^2 & \frac{1}{2}\left(dx_1^2\right)^2 \\ 1 & dx_2^1 & dx_2^2 & \frac{1}{2}\left(dx_2^1\right)^2 & dx_2^1 dx_2^2 & \frac{1}{2}\left(dx_2^2\right)^2 \\ \vdots & \vdots & \vdots & \vdots & \vdots & \vdots \\ 1 & dx_{np}^1 & dx_{np}^2 & \frac{1}{2}\left(dx_{np}^1\right)^2 & dx_{np}^1 dx_{np}^2 & \frac{1}{2}\left(dx_{np}^2\right)^2 \\ 2c & 0 & 0 & -\lambda\Delta t & 0 & -\lambda\Delta t \\ 0 & \lambda n_x & \lambda n_y & \lambda n_z & 0 & 0 \end{pmatrix}, \tag{24}$$

$$\mathbf{b} = \left[T^{\tau+1}(x_1), T^{\tau+1}(x_2), ..., T^{\tau+1}(x_{np}), 2\Delta t Q^\tau + 2cT^\tau(x) + \lambda\Delta t\nabla^2 T^\tau(x), -q_b\right]^t, \tag{25}$$

and then for the Robin boundary condition $\left(-\lambda\frac{\partial T}{\partial n} = \alpha\left(T\left(x,t\right) - T_a\right)\right)$ we have:

$$\mathbf{M} = \begin{pmatrix} 1 & dx_1^1 & dx_1^2 & \frac{1}{2}\left(dx_1^1\right)^2 & dx_1^1 dx_1^2 & \frac{1}{2}\left(dx_1^2\right)^2 \\ 1 & dx_2^1 & dx_2^2 & \frac{1}{2}\left(dx_2^1\right)^2 & dx_2^1 dx_2^2 & \frac{1}{2}\left(dx_2^2\right)^2 \\ \vdots & \vdots & \vdots & \vdots & \vdots & \vdots \\ 1 & dx_{np}^1 & dx_{np}^2 & \frac{1}{2}\left(dx_{np}^1\right)^2 & dx_{np}^1 dx_{np}^2 & \frac{1}{2}\left(dx_{np}^2\right)^2 \\ 2c & 0 & 0 & -\lambda\Delta t & 0 & -\lambda\Delta t \\ 0 & \lambda n_x & \lambda n_y & \lambda n_z & 0 & 0 \end{pmatrix}, \tag{26}$$

$$\mathbf{b} = \left[T^{\tau+1}(x_1, T^{\tau+1}(x_2), ..., T^{\tau+1}(x_{np}), 2\Delta t Q^{\tau} + 2cT^{\tau}(x) + \lambda\Delta t\nabla^2 T^{\tau}(x), \alpha T_a\right]^t. \tag{27}$$

4. Numerical examples

This study concludes with the presentation of results obtained from numerical computation. In the presented numerical computations, the simulations focus on laser irradiation using a moving beam. The values of thermo-optical and geometrical parameters of the tissue used in the simulations are shown in Table 1 (Example 1) and Table 2 (Example 2), where parameters related to the Arrhenius injury integral and the coefficients in the $G_B(\theta)$ function (10) are given in Tables 3 and 4, respectively.

Table 1. Theoretical thermo-optical and geometrical parameters – Example 1 [6].

Symbol	Parameter	Value	Unit
λ	Thermal conductivity of tissue	0.235	$\mathrm{W\cdot m^{-1}\cdot K^{-1}}$
c	Volumetric specific heat of tissue	4.284	$\mathrm{MJ\cdot m^{-3}\cdot K^{-1}}$
G_{B0}	Initial blood perfusion coefficient	0.05	$\mathrm{s^{-1}}$
μ_a	Absorption coefficient of tissue	2000	$\mathrm{m^{-1}}$
Q_{met}	Metabolic heat source	368.1	$\mathrm{W\cdot m^{-3}}$
c_B	Volumetric specific heat of blood	3.9962	$\mathrm{MJ\cdot m^{-3}\cdot K^{-1}}$
T_B	Arterial blood temperature	37	°C
L_x	Dimension along X-axis	18	mm
L_y	Dimension along Y-axis	9	mm

For the two-dimensional tissue domain, the point distribution is considered as a regular structure, generated with a spatial step of $\Delta x = \Delta y = 0.5$ mm,

TABLE 2. Theoretical thermo-optical and geometrical parameters – Example 2 [20].

Symbol	Parameter	Value	Unit
λ	Thermal conductivity of tissue	0.609	$\mathrm{W \cdot m^{-1} \cdot K^{-1}}$
c	Volumetric specific heat of tissue	4.18	$\mathrm{MJ \cdot m^{-3} \cdot K^{-1}}$
G_{B0}	Initial blood perfusion coefficient	0.00125	$\mathrm{s^{-1}}$
μ_a	Absorption coefficient of tissue	40	$\mathrm{m^{-1}}$
$\mu'_{s\,\mathrm{nat}}$	Effective scattering coefficient of native tissue	1000	$\mathrm{m^{-1}}$
$\mu'_{s\,\mathrm{den}}$	Effective scattering coefficient of destructed tissue	4000	$\mathrm{m^{-1}}$
Q_{met}	Metabolic heat source	245	$\mathrm{W \cdot m^{-3}}$
c_B	Volumetric specific heat of blood	3.9962	$\mathrm{MJ \cdot m^{-3} \cdot K^{-1}}$
T_B	Arterial blood temperature	37	°C
L_x	Dimension along X-axis	18	mm
L_y	Dimension along Y-axis	9	mm

TABLE 3. The coefficients of the perfusion coefficient function [15].

θ	m_1	m_2	m_3
$\theta = 0$	1	0	0
$0 < \theta \leq 0.1$	1	25	-260
$0.1 < \theta \leq 1$	1	-1	0
$\theta > 1$	0	0	0

TABLE 4. Arrhenius injury integral parameters [20].

Symbol	Parameter	Value	Unit
A	Pre-exponential factor	$3.1 \cdot 10^{98}$	$\mathrm{s^{-1}}$
ΔE	Activation energy	$6.27 \cdot 10^5$	$\mathrm{J \cdot mol^{-1}}$
R	Universal gas constant	8.314	$\mathrm{J \cdot mol^{-1} \cdot K^{-1}}$

while the time step Δt is set to 0.01 sec. The neighborhood radius used in the FPM, which determines the set of neighboring points is $h = 3\Delta x$, and the parameter in Eq. (19) is chosen as $\beta = 7$.

The analyzed model is supplemented by the following boundary conditions: a second type (adiabatic) condition on the tissue surface subjected to laser irradiation, while the inner tissue surfaces are assigned first-type boundary conditions with constant temperatures $T_{b1} = T_{b2} = T_{b3} = 37$°C. The initial temperature distribution is assumed as uniform at $T_0 = 37$°C. The peak laser power intensity is set to $I_0 = 1000\ \mathrm{kW \cdot m^{-2}}$, with a light reflection coefficient $Rf = 0.024$ and beam half-width $\varepsilon = 1$ mm [6].

In the presented model, the boundary conditions described in Eqs. (11)–(13) were simplified by setting constant temperature values of 37°C at the relevant

boundaries, matching the temperature typically found on the inner side of skin tissue. These values were also assumed equal across boundaries. This simplification was intended to reduce numerical complexity and to ensure consistency with the reference solution [6], thereby facilitating direct comparison of results. Since the main objective of this article is to introduce a modern meshless FPM scheme for applications in bioheat transfer, such a comparison is essential as it helps in assessing the performance of numerical methods in new application domains like the one introduced in this article. The authors acknowledge that this simplification may not fully capture real physiological conditions. However, the original algorithm description presented in the previous section enables potential readers to apply various kinds of boundary conditions and some other model modifications beyond the scope of this article. In the future, it is intended to provide a more detailed justification of boundary conditions used, or to implement more realistic, spatially varying temperature distributions where appropriate.

In the first numerical example, a comparison between the FPM and the analytical solution given in [6] is conducted. The laser beam velocity was set to 8 mm/s. In the numerical model, only the tissue absorption coefficient was taken into account ($\mu_s' = 0$), while the blood perfusion was kept constant, excluding the influence of the injury integral to maintain consistency with the input data. The values of parameters listed in Table 1 were taken for this example. In Fig. 2, the temperature computed at the central point with coordinates (9, 0) mm using both the FPM and the analytical solution is presented, focusing on the temperature rise above 37°C. It can be observed that the difference in peak temperature is only 1.29°C (FPM – 98.38°C; analytical – 99.67°C) and the difference in time is 0.085 s (FPM – 1.055 s; analytical – 1.14 s), corresponding to an error of 7.46%. This error is acceptable, especially since the tempera-

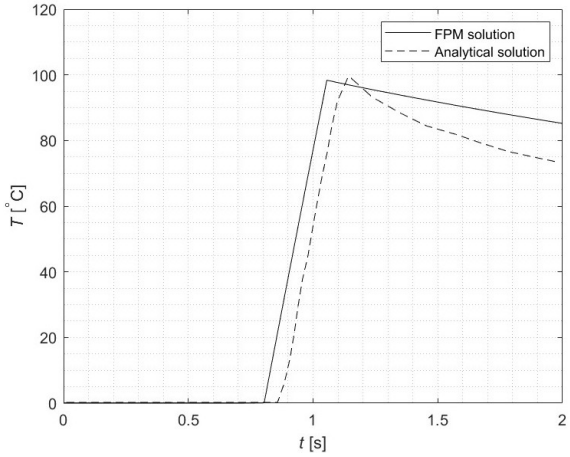

FIG. 2. Comparison of results for the central point (temperature rise profiles).

ture difference is just 1.29%. Similarly, the cooling process is slightly different, likely due to the analytical solution being formulated for a three-dimensional problems.

In the second numerical example, the laser beam velocity was set to $8\ \mathrm{mm} \cdot \mathrm{s}^{-1}$, followed by tests with various other velocities. Similarly, the peak laser power intensity was first considered as $I_0 = 1000\ \mathrm{kW} \cdot \mathrm{m}^{-2}$ and then other values were analyzed. In the numerical model, the influence of the injury integral on both blood perfusion and laser heat source is considered. The values of parameters listed in Table 2 were considered for this example.

Figure 3 depicts the profiles of both temperature and the injury integral changing in time at the central point. It can be observed that after one second, the injury integral reaches a value of 1, which means complete tissue necrosis.

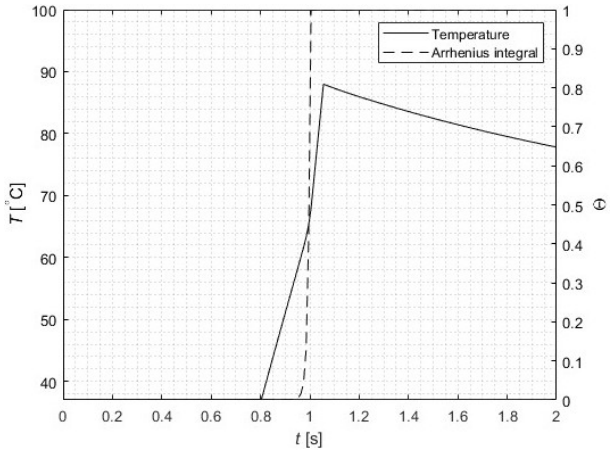

FIG. 3. Temperature and injury integral values over time at the central point.

Temperature profiles after 1, 2, 3, and 6 seconds at the tissue surface along $y = 0$ can be seen in Fig. 4. The strong influence of the first-type boundary condition can be observed here. After 2.25 seconds, when the laser beam moves out of the tissue domain, the cooling phase begins.

Figure 5 illustrates temperature changes after 2 seconds for varying laser power intensities (800, 1000, 1200 $\mathrm{kW} \cdot \mathrm{m}^{-2}$). As anticipated, higher laser powers correspond to increased maximum temperatures and deeper heat penetration. The analysis indicates that temperature dramatically decreases beyond 3 mm depth and, therefore, heat penetration past this point is minimal for each laser intensity and can be disregarded. Consequently, the laser heating process demonstrated here holds promise for treating superficial skin.

Temperature variations at the central point (9, 0) mm on the skin surface for different laser beam speeds are shown in Fig. 6. The time of observation varies for each speed, corresponding to the moment the laser beam passes over the

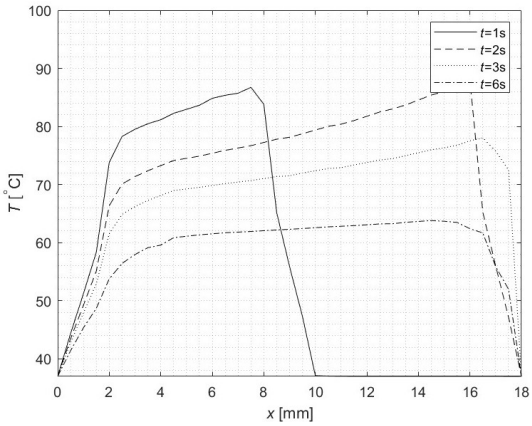

FIG. 4. Temperature profiles along the tissue surface ($y = 0$) at 1 s, 2 s, 3 s, and 6 s.

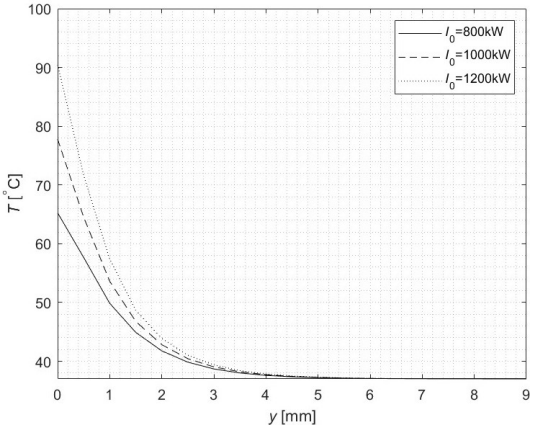

FIG. 5. Temperature values at $x = 9$ mm after 2 s for different values of I_0.

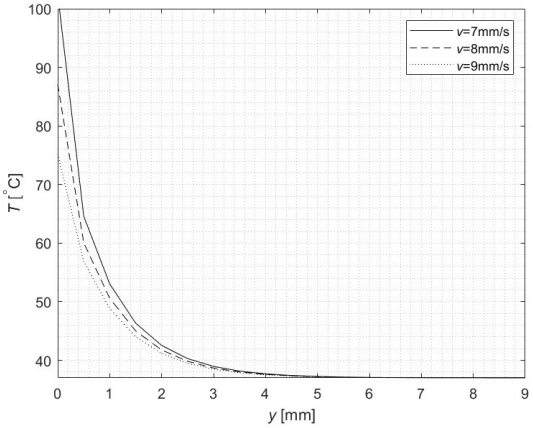

FIG. 6. Temperature values at the central point (9, 0) mm at the time moment the laser beam passes point for $x = 9$ mm for different values of v.

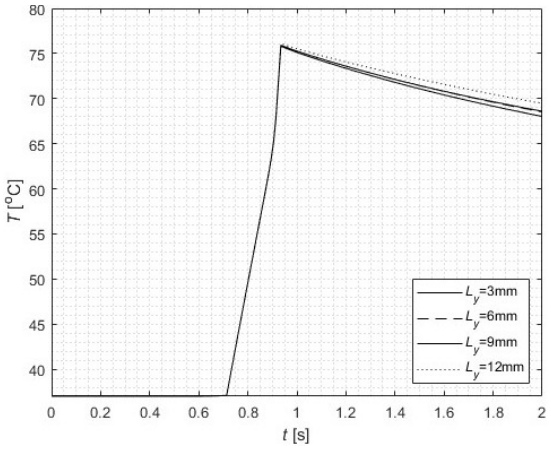

FIG. 7. Comparison of temperature rise at the central point for different L_y.

center point. A decrease in laser speed from 9 mm $\cdot$ s^{-1} to 7 mm $\cdot$ s^{-1} leads to a more pronounced temperature rise. As the speed of the laser beam increases, there is less time available for heat transfer to occur. Consequently, this leads to a reduced amount of energy being absorbed by the tissue.

Since different numerical values of thermophysical parameters can be found in the literature for the models presented, the influence of tissue thickness on temperature results is also examined and presented in Fig. 7. As shown in Fig. 7, the effect of varying tissue thickness is minimal under the conditions considered, with a peak laser power intensity of $I_0 = 800$ kW $\cdot$ m^{-2} and a laser speed of 9 mm $\cdot$ s^{-1}.

5. Conclusions

This article demonstrated the effective application of the FPM to a two-dimensional transient bioheat transfer problem involving tissue exposed to a moving laser beam.

- In the first numerical example, a comparison between the FPM and the analytical solution, assuming a constant value of blood perfusion coefficient and without considering the effective scattering coefficient, was performed. The difference in value of peak temperature was only 1.29% (1.29°C) and the difference in time was 7.46% (0.085 s). The error is acceptable, especially in temperature. The agreement of the results of both methods was satisfied, validating the accuracy of the FPM results.
- The second main mathematical model was developed based on the Pennes model by considering metabolic heat generation, a blood perfusion rate based on tissue necrosis, and a moving single-point laser beam. The ap-

plied numerical method was effective in solving complex problems involving temperature and necrosis-dependent parameters, despite being tested only on single-layer tissue, which represents some kind of a limitation of the current work. Nonetheless, this approach is a good choice for modeling dynamic thermal processes within biological tissue when subjected to laser irradiation. These simulations can assist in evaluating biological tissue damage and determining laser exposure time and intensity. Another benefit of this numerical method is its straightforward handling of boundary conditions, which opens up the potential for using it in multilayered domains or coupled problems.

- For further research, extending the model to a three-dimensional model and three-layered tissue structures is worth considering. An entirely different direction could be an application of the FPM to the dual-phase lag model. This model considers two distinct phase lag times for heat flux and temperature gradient, in contrast to the traditional Fourier heat transfer model, and thus offers a more accurate representation. The Fourier model assumes that heat waves originate from a single point within a body and rapidly propagate instantaneously throughout the material. However, this assumption does not always hold true, especially in living tissues, where heat transfer is influenced by heterogeneous tissues and blood circulation. In such scenarios, employing the dual-phase lag model can yield more realistic outcomes.

Funding

This work was supported by the National Science Centre, Poland, under the MINIATURA-7 program (DEC-2023/07/X/ST8/00564: Application of the Finite Pointset Method for numerical modeling of bioheat transport in biological tissues and solving inverse problems).

References

1. R. Verma, S. Kumar, Computational study on 2D three-phase lag bioheat model during cryosurgery using RBF meshfree method, *Journal of Thermal Biology*, **114**: 103575, 2023, https://doi.org/10.1016/j.jtherbio.2023.103575.

2. H.H. Pennes, Analysis of tissue and arterial blood temperatures in the resting human forearm, *Journal of Applied Physiology*, **1**(2): 93–122, 1948.

3. F. Xu, K.A. Seffen, T.J. Lu, Non-Fourier analysis of skin biothermomechanics, *International Journal of Heat and Mass Transfer*, **51**(9–10): 2237–2259, 2008, https://doi.org/10.1016/j.ijheatmasstransfer.2007.10.024.

4. A.D. Hobiny, I.A. Abbas, Nonlinear analysis of dual-phase lag bio-heat model in living tissues induced by laser irradiation, *Journal of Thermal Stresses*, **43**(4): 503–511, 2020, https://doi.org/10.1080/01495739.2020.1722050.

5. H. Askarizadeh, H. Ahmadikia, Analytical study on the transient heating of a two-dimensional skin tissue using parabolic and hyperbolic bioheat transfer equations, *Applied Mathematical Modelling*, **39**(13): 3704–3720, 2015, https://doi.org/10.1016/j.apm.2014.12.003.

6. B. Partovi, H. Ahmadikia, M. Mosharaf-Dehkordi, Analytical and numerical analysis of the dual-pulse lag heat transfer in a three-dimensional tissue subjected to a moving multi-point laser beam, *Journal of Thermal Biology*, **112**: 103431, 2023, https://doi.org/10.1016/j.jtherbio.2022.103431.

7. R.K. Chaudhary, I.A. Abbas, J. Singh, Numerical simulation of thermal response for non-linear multi-layer skin model subjected to heating and cooling, *Thermal Science and Engineering Progress*, **40**, 2023, https://doi.org/10.1016/j.tsep.2023.101790.

8. M. Jasiński, Modelling of thermal damage in laser irradiated tissue, *Journal of Applied Mathematics and Computational Mechanics*, **14**(4): 67–78, 2015, https://doi.org/10.17512/jamcm.2015.4.07.

9. F.R. Saucedo-Zendejo, E.O. Reséndiz-Flores, A new approach for the numerical simulation of free surface incompressible flows using a meshfree method, *Computer Methods in Applied Mechanics and Engineering*, **324**: 619–639, 2017, https://doi.org/10.1016/j.cma.2017.06.027.

10. A. Wawreńczuk, J. Kuhnert, N. Siedow, FPM computations of glass cooling with radiation, *Computer Methods in Applied Mechanics and Engineering*, **196**(45–48): 4656–4671, 2007, https://doi.org/10.1016/j.cma.2007.05.025.

11. E.O. Reséndiz-Flores, F.R. Saucedo-Zendejo, Numerical simulation of coupled fluid flow and heat transfer with phase change using the Finite Pointset Method, *International Journal of Thermal Sciences*, **133**: 13–21, 2018, https://doi.org/10.1016/j.ijthermalsci.2018.07.008.

12. F.R. Saucedo-Zendejo, E.O. Reséndiz-Flores, Meshfree numerical approach based on the Finite Pointset Method for static linear elasticity problems, *Computer Methods in Applied Mechanics and Engineering*, **372**, 2020, https://doi.org/10.1016/j.cma.2020.113367.

13. P.K. Gupta, J. Singh, K.N. Rai, S.K. Rai, Solution of the heat transfer problem in tissues during hyperthermia by finite difference-decomposition method, *Applied Mathematics and Computation*, **219**(12): 6882–6892, 2013, https://doi.org/10.1016/j.amc.2013.01.020.

14. T.N. Glenn, S. Rastegar, S.L. Jacques, Finite element analysis of temperature controlled coagulation in laser irradiated tissue, *IEEE Transactions on Biomedical Engineering*, **43**(1): 79, 1996, https://doi.org/10.1109/10.477703.

15. J.P. Abraham, E.M. Sparrow, A thermal-ablation bioheat model including liquid-to-vapor phase change, pressure- and necrosis-dependent perfusion, and moisture-dependent properties, *International Journal of Heat and Mass Transfer*, **50**: 2537–2544, 2007, https://doi.org/10.1016/j.ijheatmasstransfer.2006.11.045.

16. S. Tiwari, J. Kuhnert, Grid free method for solving the Poisson equation, *Berichte des Fraunhofer ITWM*, No. **25**, Fraunhofer Institut für Techno- und Wirtschaftsmathematik, Kaiserslautern, 2001.

17. L.J.T. Doss, N. Kousalya, Finite Pointset Method for biharmonic equations, *Computers and Mathematics with Applications*, **75**(10): 3756–3785, 2018, https://doi.org/10.1016/j.camwa.2018.02.029.

18. J. Kuhnert, *General Smoothed Particle Hydrodynamics*, Ph.D. Thesis, Technische Universität Kaiserslautern, 1999.

19. E.O. Reséndiz-Flores, I.D. García-Calvillo, Application of the finite pointset method to non-stationary heat conduction problems, *International Journal of Heat and Mass Transfer*, **71**: 720–723, 2014, https://doi.org/10.1016/j.ijheatmasstransfer.2013.12.077.

20. M. Jasiński, Numerical modeling of tissue coagulation during laser irradiation controlled by surface temperature, *Scientific Research of the Institute of Mathematics and Computer Science*, **9**(1): 29–36, 2010.

Received September 24, 2024; revised version June 9, 2025;
accepted July 7, 2025; published online July 21, 2025.